

Modulation of galactic cosmic rays during the unusual solar minimum between cycles 23 and 24

L.-L. Zhao¹, G. Qin¹, M. Zhang², and B. Heber³

L.-L. Zhao, State Key Laboratory of Space Weather, National Space Science Center, Chinese Academy of Sciences, P.O. Box 8701, Beijing 100190, China, (llzhao@spaceweather.ac.cn)

G. Qin, State Key Laboratory of Space Weather, National Space Science Center, Chinese Academy of Sciences, P.O. Box 8701, Beijing 100190, China, (gqin@spaceweather.ac.cn)

M. Zhang, Department of Physics and Space Science, Florida Institute of Technology, Melbourne, FL 32901, USA., (mzhang@fit.edu)

B. Heber, Institut für Experimentelle und Angewandte Physik, Christian-Albrechts-Universität zu Kiel, 24118 Kiel, Germany, (heber@physik.uni-kiel.de)

¹State Key Laboratory of Space Weather,
National Space Science Center, Chinese
Academy of Sciences, Beijing 100190, China

²Department of Physics and Space
Science, Florida Institute of Technology,
Melbourne, FL 32901, USA

³Institut für Experimentelle und
Angewandte Physik,

Abstract. During the recent solar minimum between cycles 23 and 24 (solar minimum $P_{23/24}$) the intensity of Galactic Cosmic Rays (GCRs) measured at the Earth was the highest ever recorded since space age. It is the purpose of this paper to resolve the most plausible mechanism for this unusually high intensity. A GCR transport model in three-dimensional heliosphere based on a simulation of Markov stochastic process is used to find the relation of cosmic ray modulation to various transport parameters, including solar wind (SW) speed, distance of heliospheric boundary, magnitude of interplanetary magnetic field (IMF) at the Earth, tilt angle of heliospheric current sheet (HCS), values of parallel and perpendicular diffusion coefficients. We calculate GCR proton energy spectra at the Earth for the last three solar minima $P_{21/22}$, $P_{22/23}$, and $P_{23/24}$, with the transport parameters obtained from observations. Besides weak IMF magnitude and slow SW speed, we find that a possible low magnetic turbulence, which increases the parallel diffusion and reduces the perpendicular diffusion in the polar direction, might be an additional possible mechanism for the high GCR intensity in the solar minimum $P_{23/24}$.

Christian-Albrechts-Universität zu Kiel,

24118 Kiel, Germany

1. Introduction

Galactic Cosmic Rays (GCRs) are energetic charged particles originated far away from the heliosphere. The high energy GCRs may reach the Earth atmosphere to produce secondary elementary particles that can be measured by ground-based Neutron Monitors (NMs) or other detectors. Although the lower energy GCRs (tens of MeV/nuc) are not usually detected by the ground-based NMs, they can be measured in space by spacecraft except during solar energetic particle (SEP) events produced by solar flares or coronal mass ejections. Unlike SEPs, GCRs form a nearly stable and isotropic background of high-energy radiation. The intensity of GCRs is slowly modulated in an anti-correlation [McDonald, 1998] with the solar activity level of 11-year cycle. It occurs because GCR particles have to travel through the magnetized interplanetary medium. The interplanetary magnetic field emanated from the Sun changes with the solar cycle, causing variations in the speed of particle transport processes such as diffusion, convection, adiabatic deceleration and drifts. Therefore, GCRs can provide important information about their propagation and modulation mechanisms in the heliosphere [Kóta, 2013]. Once the level of modulation is figured out, we can reconstruct the spectrum and composition of GCRs in the interstellar space, which can further provide information about their origin and the acceleration mechanism that produces them at the source.

The GCRs intensity measured at the Earth reached a record high level during the last solar minimum between cycles 23 and 24, noted as solar minimum $P_{23/24}$ from now on. Figure 1 shows the GCR count rates as measured by the Apatity NM, whose effective cutoff rigidity is 0.65 GV, and the monthly averaged SunSpot Numbers (SSNs) for the past

forty years. The red dashed-lines indicate the epochs of solar minima, which demarcate the solar cycles represented by the red numbers from the next ones. The black dashed-lines indicate the epochs of solar maxima, which demarcate the periods of solar magnetic polarity represented by ‘ $A > 0$ ’ or ‘ $A < 0$ ’. From Figure 1 we can clearly see a few well-known features of GCRs. First, an anti-correlation between GCR intensity and 11-year solar activity cycles is shown. Second, in the cycles with $A < 0$ magnetic polarity like 1980s, and 2000s, when the Interplanetary Magnetic Field (IMF) points towards (outwards) the Sun in the northern (southern) hemisphere [Scherer *et al.*, 2004], the time profiles of positively charged particles in the GCR are peaked, whereas the time profile is more or less flat in the cycle of $A > 0$ magnetic polarity like 1970s and 1990s. This phenomenon is attributed to the “waviness” of the Heliospheric Current Sheet (HCS) [see Kóta and Jokipii, 1983]. Besides the above characteristic behavior, we can also notice that the monthly mean SSN reached a minimum value around 2009. It was followed by a high GCR count rate which breaks the previous record February 1987 level. Meanwhile, the Solar Wind (SW) density, pressure, and IMF strength all reached the lowest values ever observed during the latest measurements made by Ulysses [Heber *et al.*, 2009].

Various models, empirical and theoretical [e.g., Ahluwalia *et al.*, 2010; Manuel *et al.*, 2011], have been used to study the unusual GCRs intensities during this solar minimum. The empirical and phenomenological GCRs modulation models are derived from observations without considering the physical processes [e.g., Nymmik *et al.*, 1992; Zhao and Qin, 2013]. But in order to understand the physical causes for such phenomenon, one needs to use theoretical models for GCR modulation. The most successful ones are based on Parker [1965], which essentially includes all important GCR modulation mechanisms such as out-

ward convection by the SW, diffusion through the irregular IMF, gradient and curvature drifts, adiabatic deceleration from the divergence of the expanding SW. *Burger and Potgieter* [1989] further concluded that GCR drift in the tilted HCS can be an important effect in solar modulation of GCR. The variation of particle perpendicular diffusion through the changes in magnetic field turbulence may also cause different levels of modulation. Recent studies also show that there is remarkable modulation in the outer heliosphere [*Scherer et al.*, 2011], probably as well as beyond the heliopause [*Strauss et al.*, 2013; *Strauss and Potgieter*, 2014]. Therefore, the GCR intensities measured at Earth is a comprehensive result of these different conditions for particle propagation through the heliosphere. More detailed theories were summarized in review papers such as *Potgieter* [1998], *Jokipii and Kóta* [2000], *Heber et al.* [2006] and *Potgieter* [2013]. Finite-difference method [*Jokipii and Kopriva*, 1979; *Kóta and Jokipii*, 1983] and stochastic method [*Zhang*, 1999; *Ball et al.*, 2005; *Pei et al.*, 2010] have been used to solve the 2-D or 3-D Parker's transport equation for GCR modulation. Calculation results were able to reproduce many observed features from measurements by spacecraft, balloon experiments, and NMs. Although the study of GCR modulation has been progressed significantly, much work still need to be done. The record level of GCR intensity during the last solar minimum naturally throw us a question: what causes the unusual solar minimum?

It is the purpose of this paper to answer the question of what causes the unusually high GCR intensity at Earth in the last solar minimum. We first present the observations of SW and IMF parameters measured at 1 AU for the last several solar cycles. Next we use a GCR transport model with numerical simulation to study the modulation of cosmic rays. Finally, through comparing our simulation results with the observations, we show what

are the possible reasons for the unusual high GCR intensity for the last solar minimum $P_{23/24}$.

2. Modulation Model

The distribution function of cosmic rays propagating through the heliosphere is governed by Parker transport equation [Parker, 1965],

$$\frac{\partial f}{\partial t} = \nabla \cdot (\kappa \cdot \nabla f) - (\mathbf{V}_{sw} + \mathbf{V}_d) \cdot \nabla f + \frac{p}{3} (\nabla \cdot \mathbf{V}_{sw}) \frac{\partial f}{\partial p}, \quad (1)$$

where $f(\mathbf{r}, p)$ is the cosmic ray distribution function, with p the particle's momentum, \mathbf{r} the particle's position, \mathbf{V}_{sw} the SW speed, and \mathbf{V}_d the gradient and curvature drifts in the IMF. The spatial diffusion coefficient tensor κ is diagonal, and consists of a parallel diffusion coefficient κ_{\parallel} and two perpendicular diffusion coefficients, $\kappa_{\perp r}$ the perpendicular diffusion coefficient in the radial direction and $\kappa_{\perp \theta}$ that in the polar direction. Here we assume the parameters are axially symmetric and time-independent on the time scale of average particle transport through the heliosphere as discussed below. In addition, we assume the IMF as a Parker spiral, and that the SW velocity is radial from the sun and constant in magnitude. Note that cosmic ray is considered isotropic, otherwise the adiabatic deceleration term, the last one in the right hand side of equation (1), has to be in the anisotropic form [e.g., Qin et al., 2004].

In this work a relatively simple spatial and momentum dependence of the diffusion coefficients is assumed following Zhang [1999] and Ferreira et al. [2001]. Firstly, parallel diffusion is set as [Zhang, 1999; Ferreira et al., 2001]

$$\kappa_{\parallel} = d\kappa_0\beta \left(\frac{p}{p_0}\right)^{\gamma} \left(\frac{B_e}{B}\right)^{\eta}, \quad (2)$$

with the parallel diffusion factor d being an adjustable constant, $\kappa_0 = 1 \times 10^{22} \text{ cm}^2 \text{ s}^{-1}$, $\gamma = 1/3$, $\eta = 1$, β is a fraction of particle's speed relative to the speed of light, $p_0 = 1 \text{ GeV c}^{-1}$ is a reference momentum, B_e is the magnetic field strength at the Earth, and B is the magnetic field at the location of the particle. Note that we set $\gamma = 1/3$ according to QLT of cosmic rays [Jokipii, 1966] for a Kolmogorov turbulence spectrum. However, other parameter from a Kraichnans scaling could also be used. Note that the form of diffusion coefficient for cosmic ray propagation in the heliosphere is rather complicated [e.g., Matthaeus et al., 2003; Qin, 2007; Shalchi et al., 2004; Zank et al., 2004]. For example, it is assumed that a break in the rigidity-dependent parallel diffusion coefficient around 4 GV is necessary for explaining the observed boron-to-carbon ratio [Büsching and Potgieter, 2008; Shalchi and Büsching, 2010]. In this work we use diffusion forms without break for the simplicity purpose. Since the peak of GCR spectrum at solar minimum is well below 1 GeV and the level of modulation is much lower for $> 4 \text{ GV}$ GCR, the effect of the break on modulated spectrum is insignificant. Secondly, the diffusion coefficients in the two perpendicular directions are set to proportional to the parallel diffusion coefficient according to test particle simulations [e.g., Giacalone and Jokipii, 1999; Qin, 2002, 2007],

$$\kappa_{\perp r} = a\kappa_{\parallel}/d = a\kappa_0\beta \left(\frac{p}{p_0}\right)^{\gamma} \left(\frac{B_e}{B}\right)^{\eta}, \quad (3)$$

with an adjustable constant factor a for the radial perpendicular diffusion, and

$$\kappa_{\perp \theta} = b\kappa_{\parallel}/d = b\kappa_0\beta \left(\frac{p}{p_0}\right)^{\gamma} \left(\frac{B_e}{B}\right)^{\eta}, \quad (4)$$

with an adjustable constant factor b for the polar diffusion perpendicular diffusion. Here, we assume different values of the parameters a and b for non-axisymmetric perpendicular diffusion because of non-axisymmetry of turbulence [e.g., Matthaeus et al., 2003] or the

background magnetic field. Note that *Effenberger et al.* [2012a] also discussed the effects of different perpendicular diffusion coefficients.

We also include a wavy HCS provided by *Jokipii and Thomas* [1981], who showed that if the solar wind velocity is radial and constant in magnitude, the HCS can be represented by

$$\theta' = \frac{\pi}{2} + \sin^{-1} \left[\sin \alpha \sin \left(\phi - \phi_0 + \frac{r\Omega}{V_{sw}} \right) \right], \quad (5)$$

where α is the HCS tilt angle (TA), ϕ_0 is an arbitrary azimuthal phase constant, and Ω is the angular velocity of the Sun's rotation corresponding to a period of 27.27 days.

Furthermore, if the TA $\alpha \ll 1$, the HCS can be approximately written as

$$\theta' \approx \frac{\pi}{2} + \alpha \sin \left(\phi - \phi_0 + \frac{r\Omega}{V_{sw}} \right). \quad (6)$$

Next, using the approximate form of HCS equation (6) we can express the Parker's spiral IMF as,

$$\mathbf{B} = \frac{A}{r^2} \left(\hat{\mathbf{e}}_r - \frac{r\Omega \sin \theta}{V_{sw}} \hat{\mathbf{e}}_\phi \right) \left[1 - 2H(\theta - \theta') \right], \quad (7)$$

where A is used to determine the strength and polarity of IMF, with pointing either outward ($A > 0$) or inward ($A < 0$) in the northern hemisphere. The Heaviside step function H is used to switch the field's direction across the HCS at $\theta = \theta'$. Note that a Fisk field with latitude-dependent solar wind speed should be used in 3D modeling, but *Hitge and Burger* [2010] found that the solar wind speed does not significantly influence cosmic ray transport in most conditions. Therefore, for the simplicity purpose, here we use Parker field with constant solar wind speed.

We describe drifts in the IMF in two different ways following *Burger and Potgieter* [1989]. Particles whose gyro motion do not cross the HCS have a pitch-angle averaged drift velocity given by the guiding center approximation. Derived with equation (7), the

regular drift velocity of a particle with charge q , momentum p , and speed v can be written as

$$\begin{aligned} \mathbf{V}_{dr} &= \frac{pv}{3q} \nabla \times \left(\frac{\mathbf{B}}{B^2} \right) \\ &= \frac{2pvr}{3qA(1 + \Gamma^2)^2} \left[-\frac{\Gamma}{\tan \theta} \hat{\mathbf{e}}_r + (2 + \Gamma^2)\Gamma \hat{\mathbf{e}}_\theta + \frac{\Gamma^2}{\tan \theta} \hat{\mathbf{e}}_\phi \right], \end{aligned} \quad (8)$$

where $\Gamma = r\Omega \sin \theta / V_{sw}$ is the tangent of the angle between the direction of IMF and the radial direction $\hat{\mathbf{e}}_r$. Particles with a trajectory that crosses the HCS will experience a fast meandering drift along the HCS. Assuming a locally flat HCS, the magnitude of the drift velocity v_{ns} along the HCS can be approximated as [see also *Burger and Potgieter, 1989*]

$$v_{ns} = \left\{ 0.457 - 0.412 \frac{d}{r_L} + 0.0915 \left(\frac{d}{r_L} \right)^2 \right\} v, \quad \text{for } |d| < 2r_L \quad (9)$$

where d is the distance from the position of the particle to the HCS, r_L is gyroradius, and v is the particle speed. Calculation results with this realistic HCS drift is the same as those with analytical HCS drift of *Kóta and Jokipii [1983]*. The direction of the HCS drift velocity is parallel to the HCS and perpendicular to the HMF ([e.g. *Burger and Potgieter, 1989*]). See *Burger [2012]* for detailed discussion on the drift velocity direction in 3-D HCS. Note that both the drift expressions (equation (8) and (9)) are only valid when scattering is neglected, which is the case for solar minimum.

The inner boundary is set at $r = 0.3$ AU as an absorption boundary. The outer boundary of the heliosphere, which assumed as the heliopause (HP) at $r = R_{HP}$, is set to be a GCR source with an assumed local interstellar spectrum (LIS)

$$J_{LIS} \propto p(m_0^2 c^2 + p^2)^{-1.8} \quad (10)$$

by following *Zhang [1999]*. Though it is believed that with measurements from Voyager 1 spacecraft in the vicinity of the heliopause [*Decker et al., 2012*] and highly accurate mea-

surements by the PAMELA mission [*Adriani et al.*, 2011], it is now possible to determine the lower limit of the very LIS for protons, helium and other ions with numerical simulations [*Herbst et al.*, 2012]. Nevertheless, the true LIS is still far from conclusive [*Webber et al.*, 2013]. In addition, different LIS models can produce the observed spectrum with LIS model-dependent modulation parameters [*Herbst et al.*, 2010]. Furthermore, recent studies show that remarkable modulation exists in the outer heliosphere and even beyond the heliopause [e.g. *Scherer et al.*, 2011; *Strauss et al.*, 2013]. And the outer heliospheric structure and boundary of the dynamic heliosphere also change associated with the varying solar activity [*Zank and Müller*, 2003; *Scherer and Fahr*, 2003; *Pogorelov et al.*, 2009]. However, assuming a steady LIS during the studied period, a distance of the boundary, and an inclusion of the heliosheath just has minor effects for modulation at 1 AU, since most of the energy loss occurs in the inner heliosphere. Here we study the modulation process within the inner heliosphere, so only the LIS without other effects over the boundary is considered for simplicity purpose.

3. Interplanetary Environment

In order to understand solar modulation of GCR with model simulations using the transport equation (1), it is important to use appropriate particle transport parameters, which are determined by the properties of the solar wind, heliospheric magnetic field, and energetic particles. Figure 2 shows the temporal evolution of IMF B_e and SW speed V_{sw} , both of which are measured at 1 AU, and the HCS TA α , for the last three solar cycles. The IMF and the SW velocity data are obtained by averaging the OMNI data over one-month intervals. And the TA of the HCS data are obtained from the WSO Web site with the “new” model. In Figure 2, we illustrate the three epochs of solar minima in

grey shadows of about half a year long as $P_{21/22}$ (1986, 91 - 1986, 273), $P_{22/23}$ (1996, 1 - 1996, 182), and $P_{23/24}$ (2009, 121 - 2009, 304). Note that all the data during the solar minima in this work are averaged over the periods shown above. From Figure 2 we can see that both the magnitude of IMF and the SW speed are very low during the recent solar minimum $P_{23/24}$, but the TA of HCS is not at the lowest level.

The solar magnetic polarity and the half year average of V_{sw} , B_e , and α during the three solar minima, which are used in our simulations for GCR modulation, are shown in the Table 1.

4. Numerical Methods

There are many approximate solutions of the Parker equation available, e.g. the most generally used force field solution [Moraal, 2013]. The appeal of the force field approach lies in the fact that observed modulation can be described with a single parameter termed modulation potential ϕ [Caballero-Lopez and Moraal, 2004]. The model assume an equilibrium between diffusion and adiabatic energy loss. Effects of drift and convection are neglected. While it is possible to reproduce the observed GCR modulation in the inner heliosphere through adjusting the modulation potential ϕ using the force field model, it cannot resolve the contribution from distinct physical mechanisms.

In this work, we use the time-backward Markov stochastic process method proposed by Zhang [1999] to solve the Parker transport equation in 3-D spherical coordinate (1). As it is more versatile and less computationally intensive, this method has been successfully implemented with different cosmic ray transport models, such as Qin *et al.* [2005] and Ball *et al.* [2005]. In this method, we trace virtual particles from the observation point back to the outer boundary with the interstellar flux expressed as equation (10). Note that the

GCR protons distribution is written as $j \sim p^2 f$. The set of SDEs, being equivalent to equation (1), for a pseudo-particle in position (r, θ, ϕ) and momentum p using spherical coordinate can be written as equation (11) [see also *Pei et al., 2010; Strauss et al., 2012*]. *Kopp et al. [2012]* and *Effenberger et al. [2012b]* also present a general discussion on the SDE technique for solving Parker transport equation.

$$\begin{aligned}
dr &= \left[\frac{1}{r^2} \frac{\partial}{\partial r} (r^2 \kappa_{rr}) + \frac{1}{r \sin \theta} \frac{\partial \kappa_{r\phi}}{\partial \phi} - V_{sw} - v_{dr} \right] ds \\
&\quad + \sqrt{2\kappa_{rr} - \frac{2\kappa_{r\phi}^2}{\kappa_{\phi\phi}}} dW_r + \frac{\sqrt{2}\kappa_{r\phi}}{\sqrt{\kappa_{\phi\phi}}} dW_\phi, \\
d\theta &= \left[\frac{1}{r^2 \sin \theta} \frac{\partial}{\partial \theta} (\sin \theta \kappa_{\theta\theta}) - \frac{v_{d\theta}}{r} \right] ds + \frac{\sqrt{2\kappa_{\theta\theta}}}{r} dW_\theta, \\
d\phi &= \left[\frac{1}{r^2 \sin^2 \theta} \frac{\partial \kappa_{\phi\phi}}{\partial \phi} + \frac{1}{r^2 \sin \theta} \frac{\partial}{\partial r} (r \kappa_{r\phi}) - \frac{v_{d\phi}}{r \sin \theta} \right] ds \\
&\quad + \frac{\sqrt{2\kappa_{\phi\phi}}}{r \sin \theta} dW_\phi, \\
dp &= \frac{p}{3r^2} \frac{\partial r^2 V_{sw}}{\partial r} ds.
\end{aligned} \tag{11}$$

Using the stochastic simulation, we can obtain not only modulated GCRs fluxes, but also the behavior of individual particle, e.g. the propagation time and energy loss [*Strauss et al., 2011*]. In addition, we can incorporate almost any kind of magnetic field configuration according to observations or MHD numerical simulations [*Strauss et al., 2013*]. Furthermore, this stochastic numerical method is more computationally efficient than the traditional finite difference approach, with the added advantage that it is easy to parallelize. Note that the integration of stochastic differential equation is performed in terms of spherical coordinates, which further [enhances](#) the computational efficiency by reducing coordinate transformations.

5. Modulation Effects

In this section the effects of various transport parameters on GCR modulation are discussed. Throughout this section, we set magnitude of IMF at 1 AU $B_e = 5$ nT, SW speed $V_{sw} = 400$ km/s, TA of HCS $\alpha = 0^\circ$, and heliospheric outer boundary distance as 80 AU, unless otherwise stated. Note that all results from numerical simulations and observations are at 1 AU in the ecliptic.

5.1. Modulation Effects of Interplanetary Parameters

First, we study the modulation effects of interplanetary solar wind and magnetic field parameters. In these simulations, we set diffusion factors $a = 0.03$, $b = 0.01$ and $d = 1$ in equations (3), (4) and (2), respectively. The TA of HCS is set to $\alpha = 0^\circ$ which is appropriate for the solar minimum condition. Figure 3 illustrates separately the computed differential intensity for GCR protons with different interplanetary parameters used in this study. The calculations are done for both solar magnetic polarities. The top panels of each figure show the results in the $A > 0$ epochs, and the bottom panels show the results in the $A < 0$ epochs, with the interstellar unmodulated spectrum (grey lines) for reference.

Figure 3(a) shows the influence of different SW speeds on GCR proton intensity, with the dark solid, dotted, and dashed lines representing three assumptions of SW speed, 300 km/s, 400 km/s, and 500 km/s, respectively. Although the IMF magnitude at the Earth B_e is fixed, the magnetic field magnitude in the heliosphere is dependent on the SW speed and varies according to equation (7). We can see there is an obvious anti-correlation between SW speed and GCR intensity. Figure 3(b) illustrates the influence of the heliospheric outer boundary radial distance on GCR intensity, with the dark solid, dotted, and dashed lines representing three assumptions for the outer boundary radial

distance, 60 AU, 80 AU, and 100 AU, respectively. We can see that the outer boundary radial distance has little effect on the GCR flux measured at 1 AU, no matter whether $A > 0$ or $A < 0$. In Figure 3(c) the computed GCR proton intensities for different magnitude of IMF at 1 AU are shown. Compared with the results of SW speed and outer heliospheric boundary, the increased magnitude of IMF remarkably declines the GCR intensity for both magnetic epochs, especially for the lower energy range.

Overall, Figure 3 suggests that, in our model, the low SW speed and magnitude of IMF play significant role in increasing the GCR flux, while the effect of outer heliospheric boundary is negligible. Therefore, we set the outer heliospheric boundary distance as 80 AU in the rest of the paper, but the SW speed and magnitude of IMF for each period according to the Table 1.

In order to show the effectiveness of lower SW speed and magnitude of IMF on the significant increase of GCR intensity in the recent extreme solar minimum, we calculate GCR intensities with interplanetary properties during each of the last three solar minima shown in Figure 4. Here, we set SW speed V_{sw} and IMF magnitude at the Earth B_e during the last three solar minima as that in the Table 1. In Figure 4(a), by setting TA of HCS as 0, we find that the GCR intensity during $P_{23/24}$ increases significantly. However, in Figure 4(b), by setting TA of HCS for different solar minima as shown in Table 1, the increase of the GCR intensity during $P_{23/24}$ is less prominent compared with the spacecraft measurements shown later. Although the particle drifts, including the global gradient and curvature drifts, still play a significant role in CR modulation, the fact that the TA of HCS during $P_{23/24}$ is not the lowest prevent us from reproducing the abnormally high

GCR intensity. So we need to consider the other physical mechanisms of modulation processes.

5.2. Modulation Effects of Diffusion Coefficients

Since during the extreme solar minimum $P_{23/24}$, an $A < 0$ epoch, the solar activity was unusually quiet compared to that in the other solar minima, with an expected lower turbulence level in solar wind, both the radial and polar perpendicular diffusion coefficients, $\kappa_{\perp r}$ and $\kappa_{\perp \theta}$, respectively, became smaller, and the parallel diffusion coefficient, κ_{\parallel} , became larger. Here, we investigate the effects of polar perpendicular diffusion factor b , radial perpendicular diffusion factor a , and parallel diffusion factor d , on the GCR intensity, especially during an $A < 0$ epoch (Figure 5). It is similar to *Reinecke and Potgieter* [1993] who discussed different diffusion coefficients on the different intensity of CR during consecutive solar minimum. Following *Effenberger et al.* [2012a], we also use an anisotropic diffusion coefficients in this study. In these simulations, we set diffusion factors $a = 0.03$, $b = 0.01$ and $d = 1$ in equations (3), (4) and (2), respectively, unless otherwise stated.

The modulation effectiveness of $\kappa_{\perp \theta}$ for both magnetic epochs, $A > 0$ and $A < 0$, is illustrated in Figure 5(a). Simulation results with $b = 0.01$, $b = 0.03$, and $b = 0.05$ are shown with dark solid, dotted, and dashed lines, respectively. While a lower polar perpendicular diffusion factor b has little effect on the GCRs intensity in the $A > 0$ epochs, it can significantly increase GCRs intensity in the $A < 0$ epochs. Moreover, Figure 5(b) and 5(c) show that higher radial perpendicular diffusion factor a and parallel diffusion factor d can increase GCRs intensity slightly for both solar epochs. Nevertheless, this

effect can be significantly weakened by an decrease of polar perpendicular diffusion factor b .

The above study shows that the decrease of b can cause the increase of GCR intensity. In an $A < 0$ epoch, this influence is more effective than the factor a and d . Therefore, it is possible to use the combined effect of these transport parameters to explain the record level of GCR flux in $P_{23/24}$ solar minimum. Note that, in the following simulation, the values of magnetic field magnitude B_e , solar wind speed V_{sw} , and tilt angle of current sheet α are from measurements, but the diffusion factors a , b , and d are free parameters constrained by fitting numerical simulation results to the spacecraft measurements.

6. GCRs Data

In this paper, we use GCRs data from both ground based NM count rates and proton flux of spacecraft measurements. The GCR data are obtained with half year average for each of three solar minimum, $P_{21/22}$, $P_{22/23}$, and $P_{23/24}$.

The NM stations we use for GCRs data are Apatity, Oulu, Yakutsk, Moscow, Novosibirsk, Lomnický štít, Jungfraujoch, Hermanus, Rome, Tbilisi, and Potchefstroom NMs. In order to compare GCRs count rates measured by NMs with flux from simulation results, we use the effective energy of each NM [Alanko *et al.*, 2003], which can be approximated as

$$E_{\text{eff}} = E_1 + \frac{E_2 (P_c/P_1)^{1.25}}{1 + 10 \exp(-0.45P_c/P_1)}, \quad (12)$$

where P_c is the local geomagnetic cutoff rigidity, $E_1 = 6.4$ GeV, $E_2 = 1.45$ GeV, and $P_1 = 1$ GV. Thus the integral GCR flux above the effective energy $M(E_{\text{eff}})$ is defined as

$$M(E_{\text{eff}}) = \int_{E_{\text{eff}}}^{\infty} j(E) d(E) \quad (13)$$

is directly proportional to the NM count rates, or

$$M(E_{\text{eff}}) = K_{\text{NM}}N(P_c), \quad (14)$$

with $N(P_c)$ the NM count rates, and K_{NM} a constant for any NM. Therefore, for different NMs we can compare the computed $M(E_{\text{eff}})$ with observational data of the NM count rates. Note that the effective energy is quite different from the median rigidity below which lies 50% of detector counting rate [?], widely used for transient cosmic ray solar modulation studies [?].

Table 2 shows the local geomagnetic cutoff rigidity P_c , and the corresponding effective energy E_{eff} of NMs used in our work.

The data are obtained from STEREO and PAMELA for energy 22 ~ 77 MeV and 82 ~ 20,000 MeV, respectively, during the period $P_{23/24}$, and IMP-8 for energy 70 ~ 400 MeV during the periods $P_{21/22}$ and $P_{22/23}$. The data of IMP-8 and STEREO contain both GCRs and SEPs. It is assumed that the modulated GCRs flux can be described as a stable “background”, while SEPs appear typically as short spikes of a few days long except for relative higher energy particles. Therefore, similar to what was done in *Qin et al.* [2012] we use an automatic despiking algorithm based on Poincaré map thresholding method [*Goring and Nikora, 2002*] to remove the SEP spikes for STEREO and IMP-8 data. For more details to remove the SEP contamination in the time-series GCR flux from spacecraft observations, please refer to *Qin et al.* [2012].

7. Simulation Results

In the following we compare the results of our numerical simulation of GCR spectra with measurements to find out possible reasons for the unusually high cosmic ray intensity during the $P_{23/24}$ solar minimum.

Figure 6 shows the computed GCRs of protons energy spectra at the Earth for the last three solar minima with interplanetary parameters from observations shown in Table 1, which include the solar magnetic polarity, magnitude of IMF, SW speed, TA of HCS. As a reference, black solid line indicates the unmodulated GCR spectrum at the outer boundary. Lines shown in purple, black, and red colors represent $P_{21/22}$, $P_{22/23}$, and $P_{23/24}$, respectively. IMP-8 and STEREO spacecraft measurements of GCRs are shown as diamonds and squares, respectively, and red circles denote the measurements from PAMELA instrument in the higher energy range for the year 2009 [Adriani *et al.*, 2013, Table 1]. For each energy point, the flux is calculated with a stochastic process simulation. From Figure 6 we can see that with diffusion parameters $a = 0.03$, $b = 0.02$, and $d = 0.5$, the simulation results fit well to the IMP-8 observational data during $P_{21/22}$ and $P_{22/23}$. As discussed earlier, in the solar minimum $P_{23/24}$ the solar activity was extremely quiet, so that the particles perpendicular diffusion coefficients are set to be smaller, and that the particles parallel diffusion coefficients are larger. For this reason, in $P_{23/24}$ the parameters a and b should be smaller and the parameter d should be larger. From Figure 6 it is shown that with parameters $a = 0.02$, $b = 0.01$, and $d = 1$, and other parameters set as in Table 1, the simulation results fit well to the observations from both STEREO and PAMELA during the solar minimum $P_{23/24}$.

Figure 7 shows a comparison of the integral intensity $M(E)$ as a function of GCR energy E between our simulation results and the NM measurements. Similar to Figure 6, the black solid line indicates the unmodulated GCR spectrum, and the three lines in different colors represent our calculations for the three solar minima. Note that both simulation result and observation of each solar minimum are multiplied by an arbitrary factor for the purpose of presentation. For each NM with a cutoff rigidity P_c given in Table 2, we have calculated $M(E_{\text{eff}})$ (colored lines) as an integration of simulated GCR flux $j(E)$ using equation (13). In order to make a direct comparison between $M(E_{\text{eff}})$ from our simulation results (green line) and the NM count rates in $P_{21/22}$, we obtain a normalization constant K_{NM} with equation (14) for each NM, and we show the K_{NM} in Table 2. With the K_{NM} we can convert all NMs' count rates $N(P_c)$ to their $M(E_{\text{NM}})$, which is denoted as observational data (color dots) for periods other than $P_{21/22}$. Note that the constants K_{NM} are obtained with equation (14) for data in $P_{21/22}$, so the green dots agree with green line exactly for $P_{21/22}$. For the other two solar minima, we use the same normalization constant and NM measurements to obtain the blue and red dots, which are considered as measurements. Therefore, the fact that the blue and red dots agree well with blue and red lines, respectively, show that our simulation results fit well with the NMs count rates for periods $P_{22/23}$ and $P_{23/24}$. We especially point out that in $P_{23/24}$, the NMs count rates were much higher than previous solar minima and our simulations reproduce such a phenomenon.

Furthermore, we study the evolution of the proton energy spectrum during the period of the solar minimum $P_{23/24}$ (Figure 8). The proton flux measurements from PAMELA instrument with monthly average [Adriani *et al.*, 2013, table 1] for year 2007, 2008 and

2009 are represented with purple, blue and red circles respectively. Obviously, the proton spectra in 2009 represents the highest flux observed. Figure 8 also shows the computed differential intensity of GCR protons at the Earth from 2007 to 2009 (solid lines) in half year periods. For simulations in these half year periods, the SW speed, magnitude of IMF and TA of HCS are from the averaged observations, while the diffusion coefficient parameters a , b , and d are the same as the $P_{23/24}$ solar minimum. We can see that the simulation results agree well with PAMELA measurements.

8. Discussion

In this study, we investigate the behaviors of GCR modulation at Earth and try to determine the potential mechanisms responsible for the abnormally high GCR intensity in the last solar minimum, through comparing the numerical simulation results with the observations from NM stations and spacecraft instruments.

Various modulation processes could contribute to the high GCR intensity, e.g., particle drifts, diffusion, or possible weaken outer heliosphere modulation. Generally, drifts effects are thought to dominant modulation process at solar minimum for $A < 0$ epochs [Kóta and Jokipii, 1983]. Cliver *et al.* [2013] argues that diffusion is the primary modulation process during this unusual solar minimum. Potgieter *et al.* [2014] also shows that the rigidity-dependent diffusion coefficients need to decrease significantly below ~ 3 GeV to reproduce the proton spectra from PAMELA experiment. In this work, we further highlight that a possible low magnetic turbulence, which increases the parallel diffusion and reduces the perpendicular diffusion in the polar direction, might be an additional mechanism for the high GCR intensity during the $P_{23/24}$ solar minimum.

Energetic particles can be scattered parallel to the background magnetic field because of magnetic turbulence, so higher turbulence levels would cause stronger scattering and shorter parallel mean free path. In addition, energetic particles perpendicular diffusion is achieved with the diffusive separate of particle gyrocenters caused by turbulence transverse complexity. Therefore, lower turbulence levels would increase parallel diffusion and decrease perpendicular diffusion [e.g., Jokipii, 1966; Matthaeus et al., 2003; Qin, 2007].

However, drifts still play a significant role in the modulation process, even though the 2009 solar minimum is more ‘diffusion dominated’ than previous solar minima [Potgieter et al., 2014]. A low SW speed can cause less outward convection of GCRs out of the heliosphere and less adiabatic cooling, and a low magnitude of IMF would cause much increase of particle drift according to equation (8) in our model and diffusion. In fact, the more realistic scenario is that all modulation processes interplay dynamically, contributing to the observed increases in the proton spectra.

We can use the most advanced NLGC theory for the diffusion coefficients[e.g., NLGC, Matthaeus et al., 2003]. The theory depends on assumption of turbulence type and its transport. Many free parameters are need in this theory. In this work, we assume ad hoc changes in the magnitude of diffusion coefficients. And our parameters only give a sense how the diffusion coefficients are expected to be.

Furthermore, the varies of magnetic turbulence properties, such as turbulence levels and turbulence correlation scales are important to cause the changes in diffusion coefficients. Nevertheless, since there is no in-situ measurement of diffusion coefficients, it is very difficult to estimate the diffusion coefficients quantitatively via comparing simulation results with the observations. Generally, there are two ways to address this issue. On the one

hand, more realistic and accurate 3-D heliospheric model should be implemented in the simulation process, e.g., solar wind profile and IMF structure from 3-D MHD numerical simulation, as well as GCR drift model within 3-D HCS structure. Moreover, modulation in the outer heliosphere should also be taken into account. On the other hand, more observations should be used to verify this hypothesis. For instance, the electron and positron spectra observed by PAMELA provides us an unprecedented opportunity to further investigate the modulation process in this unusual solar minimum, and the high statistically significant fluxes of heavy-ions from ACE spacecraft also help to constrain the modulation model more strictly. However, these topics are out of the scope of this paper, and we leave them for future study.

9. Conclusions

Observations of GCR count rates of NMs and the transport parameters from spacecraft measurements for the last three solar cycles show that during the solar minimum $P_{23/24}$, the intensity of GCRs was the highest, while the IMF and the SW speed were both weaker than the previous two solar minima, $P_{21/22}$ and $P_{22/23}$, but the TA of HCS was not at the lowest level. We first study modulation effects of the related transport parameters during the solar minimum separately, including SW speed, outer heliospheric boundary, magnitude of IMF at the Earth, and parallel and perpendicular diffusion coefficients. Despite the fact that drifts still play a significant role in the modulation process, we find that the particle drift during this $A < 0$ cycle cannot contribute solely to the high flux of GCRs in the recent solar minimum $P_{23/24}$. Furthermore, during the recent solar minimum $P_{23/24}$ the solar activity was very weak and solar wind turbulence level was expected to be lower than previous solar minima, so that particles radial and polar perpendicular

diffusion coefficients should be smaller and parallel diffusion coefficients should be larger. Therefore, we have to further tune the magnitude of diffusion coefficients. It is found that a lower polar perpendicular diffusion with factor b can cause the increase of GCRs intensity. In addition, the factor b is more effective than the radial perpendicular diffusion factor a and parallel diffusion factor d for the $A < 0$ cycle. The combination of lower polar diffusion coefficient, higher parallel diffusion coefficient, lower SW speed, and lower magnetic field in the solar minimum $P_{23/24}$ is possible to explain the unusually high GCR intensity.

Although relatively simple models are implemented in our simulation model, this work represents an important first step towards investigating the unusual cosmic ray modulation during the last solar minimum quantitatively. Further effort is needed to overcome these limitations in a more comprehensive way.

Acknowledgments. This work was supported in part by grants NNSFC 41125016, NNSFC 41374177, CMA grant GYHY201106011, and the Specialized Research Fund for State Key Laboratories of China. The computations were performed by Numerical Forecast Modeling R&D and VR System of State Key Laboratory of Space Weather and Special HPC work stand of Chinese Meridian Project. We benefited from the Sunspot data provided by SIDC Team 2009, the Wilcox Solar Observatory data obtained via the web site <http://wso.stanford.edu>, energetic particle data provided by IMP-8 Goddard Medium Energy (GME) Experiment, STEREO High Energy Telescope (HET). We are grateful to the SPDF OMNIWeb interface at <http://omniweb.gsfc.nasa.gov> for the solar and interplanetary data. We also thank the providers of NM data used in this study.

References

- Adriani, O., et al. (2011), PAMELA measurements of cosmic-ray proton and helium spectra, *Science*, *332*(6025), 69–72, doi:10.1126/science.1199172.
- Adriani, O., et al. (2013), Time eependence of the proton flux measured by PAMELA during the 2006 July-2009 December solar minimum, *Astrophys. J.*, *765*, 91, doi: 10.1088/0004-637X/765/2/91.
- Ahluwalia, H. S., C. Lopate, R. C. Ygbuhay, and M. L. Duldig (2010), Galactic cosmic ray modulation for sunspot cycle 23, *Adv. Space Res.*, *46*(7), 934 – 941, doi: <http://dx.doi.org/10.1016/j.asr.2010.04.008>.
- Alanko, K., I. G. Usoskin, K. Mursula, and G. A. Kovaltsov (2003), Heliospheric modulation strength: effective neutron monitor energy, *Adv. Space Res.*, *32*(4), 615–620, doi:10.1016/S0273-1177(03)00348-X.
- Ball, B., M. Zhang, H. Rassoul, and T. Linde (2005), Galactic cosmic-ray modulation using a solar minimum MHD heliosphere: a stochastic particle approach, *Astrophys. J.*, *634*(2), 1116, doi:10.1086/496965.
- Burger, R. A. (2012), Modeling drift along the heliospheric wavy neutral sheet, *Astrophys. J.*, *760*(1), 60, doi:10.1088/0004-637X/760/1/60.
- Burger, R. A., and M. S. Potgieter (1989), The calculation of neutral sheet drift in two-dimensional cosmic-ray modulation models, *Astrophys. J.*, *339*, 501–511, doi: 10.1086/167313.
- Büsching, I., and M. S. Potgieter (2008), The variability of the proton cosmic ray flux on the Sun’s way around the galactic center, *Adv. Space Res.*, *42*, 504–509, doi: 10.1016/j.asr.2007.05.051.

- Caballero-Lopez, R. A., and H. Moraal (2004), Limitations of the force field equation to describe cosmic ray modulation, *J. Geophys. Res.*, *109*, A01101, doi:10.1029/2003JA010098.
- Cliver, E. W., I. G. Richardson, and A. G. Ling (2013), Solar Drivers of 11-yr and Long-Term Cosmic Ray Modulation, *Space Sci. Rev.*, *176*, 3–19, doi:10.1007/s11214-011-9746-3.
- Decker, R. B., S. M. Krimigis, E. C. Roelof, and M. E. Hill (2012), No meridional plasma flow in the heliosheath transition region, *Nature*, *489*, 124–127, doi:10.1038/nature11441.
- Effenberger, F., H. Fichtner, K. Scherer, S. Barra, J. Kleimann, and R. D. Strauss (2012a), A generalized diffusion tensor for fully anisotropic diffusion of energetic particles in the heliospheric magnetic field, *Astrophys. J.*, *750*, 108, doi:10.1088/0004-637X/750/2/108.
- Effenberger, F., H. Fichtner, K. Scherer, and I. Büsching (2012b), Anisotropic diffusion of galactic cosmic ray protons and their steady-state azimuthal distribution, *Astrophys. J.*, *547*, A120, doi:10.1051/0004-6361/201220203.
- Ferreira, S. E. S., M. S. Potgieter, R. A. Burger, B. Heber, and H. Fichtner (2001), Modulation of Jovian and galactic electrons in the heliosphere: 1. Latitudinal transport of a few MeV electrons, *J. Geophys. Res.*, *106*, 24,979–24,988, doi:10.1029/2001JA000082.
- Giacalone, J., and J. R. Jokipii (1999), The transport of cosmic rays across a turbulent magnetic field, *Astrophys. J.*, *520*, 204–214, doi:10.1086/307452.
- Goring, D., and V. Nikora (2002), Despiking acoustic doppler velocimeter data, *J. Hydraul. Eng.*, *128*(1), 117–126, doi:10.1061/(ASCE)0733-9429(2002)128:1(117).

- Heber, B., H. Fichtner, and K. Scherer (2006), Solar and heliospheric modulation of galactic cosmic rays, *Space Sci. Rev.*, *125*, 81–93, doi:10.1007/s11214-006-9048-3.
- Heber, B., A. Kopp, J. Gieseler, R. Müller-Mellin, H. Fichtner, K. Scherer, M. S. Potgieter, and S. E. S. Ferreira (2009), Modulation of galactic cosmic ray protons and electrons during an unusual solar minimum, *Astrophys. J.*, *699*, 1956–1963, doi:10.1088/0004-637X/699/2/1956.
- Herbst, K., A. Kopp, B. Heber, F. Steinhilber, H. Fichtner, K. Scherer, and D. Matthiä (2010), On the importance of the local interstellar spectrum for the solar modulation parameter, *J. Geophys. Res.*, *115*, D00I20, doi:10.1029/2009JD012557.
- Herbst, K., B. Heber, A. Kopp, O. Sternal, and F. Steinhilber (2012), The local interstellar spectrum beyond the heliopause: what can be learned from Voyager in the inner heliosheath?, *Astrophys. J.*, *761*, 17, doi:10.1088/0004-637X/761/1/17.
- Hitge, M., and R. A. Burger (2010), Cosmic ray modulation with a Fisk-type heliospheric magnetic field and a latitude-dependent solar wind speed, *Adv. Space Res.*, *45*, 18–27, doi:10.1016/j.asr.2009.07.024.
- Jokipii, J. R. (1966), Cosmic-ray propagation. I. charged particles in a random magnetic field, *Astrophys. J.*, *146*, 480, doi:10.1086/148912.
- Jokipii, J. R., and D. A. Kopriva (1979), Effects of particle drift on the transport of cosmic rays. III - Numerical models of galactic cosmic-ray modulation, *Astrophys. J.*, *234*, 384–392, doi:10.1086/157506.
- Jokipii, J. R., and J. Kóta (2000), Galactic and anomalous cosmic rays in the heliosphere, *Astrophys. Space Sci.*, *274*, 77–96, doi:10.1023/A:1026535603934.

- Jokipii, J. R., and B. Thomas (1981), Effects of drift on the transport of cosmic rays. IV - Modulation by a wavy interplanetary current sheet, *Astrophys. J.*, *243*, 1115–1122, doi:10.1086/158675.
- Kopp, A., I. Büsching, R. D. Strauss, and M. S. Potgieter (2012), A stochastic differential equation code for multidimensional Fokker-Planck type problems, *Comput. Phys. Commun.*, *183*, 530–542, doi:10.1016/j.cpc.2011.11.014.
- Kóta, J. (2013), Theory and modeling of galactic cosmic rays: trends and prospects, *Space. Sci. Rev.*, *176*, 391–403, doi:10.1007/s11214-012-9870-8.
- Kóta, J., and J. R. Jokipii (1983), Effects of drift on the transport of cosmic rays. VI - a three-dimensional model including diffusion, *Astrophys. J.*, *265*, 573–581, doi:10.1086/160701.
- Manuel, R., S. E. S. Ferreira, M. S. Potgieter, R. D. Strauss, and N. E. Engelbrecht (2011), Time-dependent cosmic ray modulation, *Adv. Space Res.*, *47*(9), 1529 – 1537, doi:10.1016/j.asr.2010.12.007.
- Matthaeus, W. H., G. Qin, J. W. Bieber, and G. P. Zank (2003), Nonlinear collisionless perpendicular diffusion of charged particles, *Astrophys. J.*, *590*, L53–L56, doi:10.1086/376613.
- McDonald, F. B. (1998), Cosmic-ray modulation in the heliosphere—a phenomenological study, *Space Sci. Rev.*, *83*, 33–50, doi:10.1023/A:1005052908493.
- Moraal, H. (2013), Cosmic-Ray Modulation Equations, *Space Sci. Rev.*, *176*, 299–319, doi:10.1007/s11214-011-9819-3.
- Nymmik, R. A., M. I. Panasyuk, T. I. Pervaja, and A. A. Suslov (1992), A model of galactic cosmic ray fluxes, *Int. J. Rad. Appl. Instrum. Part D. Nucl. Track. Radiat.*

Meas., 20(3), 427–429, doi:[http://dx.doi.org/10.1016/1359-0189\(92\)90028-T](http://dx.doi.org/10.1016/1359-0189(92)90028-T).

Parker, E. N. (1965), The passage of energetic charged particles through interplanetary space, *Planet. Space Sci.*, 13, 9–49, doi:10.1016/0032-0633(65)90131-5.

Pei, C., J. W. Bieber, R. A. Burger, and J. Clem (2010), A general time-dependent stochastic method for solving parker’s transport equation in spherical coordinates, *J. Geophys. Res.*, 115(A12), A12,107.

Pogorelov, N. V., J. Heerikhuisen, G. P. Zank, and S. N. Borovikov (2009), Influence of the interstellar magnetic field and neutrals on the shape of the outer heliosphere, *Space Sci. Rev.*, 143, 31–42, doi:10.1007/s11214-008-9429-x.

Potgieter, M. (2013), Solar modulation of cosmic rays, *Living Rev. Solar Phys.*, 10, 3, doi:10.12942/lrsp-2013-3.

Potgieter, M. S. (1998), The modulation of galactic cosmic rays in the heliosphere: theory and models, *Space Sci. Rev.*, 83(1), 147–158, doi:10.1023/A:1005014722123.

Potgieter, M. S., E. E. Vos, M. Boezio, N. De Simone, V. Di Felice, and V. Formato (2014), Modulation of Galactic Protons in the Heliosphere During the Unusual Solar Minimum of 2006 to 2009, *Solar Phys.*, 289, 391–406, doi:10.1007/s11207-013-0324-6.

Qin, G. (2002), Charged particle transport in magnetic field turbulence and study of trim simulation and SSX experiment, Ph.D. thesis, University of Delaware.

Qin, G. (2007), Nonlinear parallel diffusion of charged particles: extension to the nonlinear guiding center theory, *Astrophys. J.*, 656, 217–221, doi:10.1086/510510.

Qin, G., M. Zhang, J. R. Dwyer, and H. K. Rassoul (2004), Interplanetary transport mechanisms of solar energetic particles, *Astrophys. J.*, 609, 1076–1081, doi:10.1086/421101.

- Qin, G., M. Zhang, J. R. Dwyer, H. K. Rassoul, and G. M. Mason (2005), The model dependence of solar energetic particle mean free paths under weak scattering, *Astrophys. J.*, *627*, 562–566, doi:10.1086/430136.
- Qin, G., L.-L. Zhao, and H.-C. Chen (2012), Despiking of spacecraft energetic proton flux to study galactic cosmic-ray modulation, *Astrophys. J.*, *752*(2), 138, doi:10.1088/0004-637X/752/2/138.
- Reinecke, J. P. L., and M. S. Potgieter (1993), An explanation for the observed intersection of cosmic-ray spectra for consecutive solar minimum periods, *Int. Cosmic Ray Conf.*, *3*, 597.
- Scherer, K., and H. J. Fahr (2003), Solar cycle induced variations of the outer heliospheric structures, *Geophys. Res. Lett.*, *30*(2), 1045, doi:10.1029/2002GL016073.
- Scherer, K., H.-J. Fahr, H. Fichtner, and B. Heber (2004), Long-term modulation of cosmic rays in the heliosphere and its influence at earth, *Solar Phys.*, *224*, 305–316, doi:10.1007/s11207-005-5687-x.
- Scherer, K., H. Fichtner, R. D. Strauss, S. E. S. Ferreira, M. S. Potgieter, and H.-J. Fahr (2011), On cosmic ray modulation beyond the heliopause: where is the modulation boundary?, *Astrophys. J.*, *735*, 128, doi:10.1088/0004-637X/735/2/128.
- Shalchi, A., and I. Büsching (2010), Influence of turbulence dissipation effects on the propagation of low-energy cosmic rays in the galaxy, *Astrophys. J.*, *725*, 2110–2116, doi:10.1088/0004-637X/725/2/2110.
- Shalchi, A., J. W. Bieber, and W. H. Matthaeus (2004), Analytic forms of the perpendicular diffusion coefficient in magnetostatic turbulence, *Astrophys. J.*, *604*, 675–686, doi:10.1086/382128.

- Strauss, R. D., and M. S. Potgieter (2014), Where does the heliospheric modulation of galactic cosmic rays start?, *Adv. Space Res.*, doi:<http://dx.doi.org/10.1016/j.asr.2014.01.004>.
- Strauss, R. D., M. S. Potgieter, A. Kopp, and I. Büsching (2011), On the propagation times and energy losses of cosmic rays in the heliosphere, *J. Geophys. Res.*, *116*, A12105, doi:10.1029/2011JA016831.
- Strauss, R. D., M. S. Potgieter, I. Büsching, and A. Kopp (2012), Modelling heliospheric current sheet drift in stochastic cosmic ray transport models, *Astrophys. Space Sci.*, *339*, 223–236, doi:10.1007/s10509-012-1003-z.
- Strauss, R. D., M. S. Potgieter, S. E. S. Ferreira, H. Fichtner, and K. Scherer (2013), Cosmic ray modulation beyond the heliopause: a hybrid modeling approach, *Astrophys. J. Lett.*, *765*, L18, doi:10.1088/2041-8205/765/1/L18.
- Webber, W. R., P. R. Higbie, and F. B. McDonald (2013), The unfolding of the spectra of low energy galactic cosmic ray H and He nuclei as the Voyager 1 spacecraft exits the region of heliospheric modulation, *ArXiv e-prints*.
- Zank, G. P., and H.-R. Müller (2003), The dynamical heliosphere, *J. Geophys. Res.*, *108*, 1240, doi:10.1029/2002JA009689.
- Zank, G. P., G. Li, V. Florinski, W. H. Matthaeus, G. M. Webb, and J. A. Le Roux (2004), Perpendicular diffusion coefficient for charged particles of arbitrary energy, *J. Geophys. Res.*, *109*, A04107, doi:10.1029/2003JA010301.
- Zhang, M. (1999), A markov stochastic process theory of cosmic-ray modulation, *Astrophys. J.*, *513*, 409–420, doi:10.1086/306857.

Zhao, L.-L., and G. Qin (2013), An observation-based GCR model of heavy nuclei: measurements from CRIS onboard ACE spacecraft, *J. Geophys. Res.*, pp. 1837–1848, doi: 10.1002/jgra.50235.

Table 1. Values of parameters used in the simulations for the last three solar minima.

Parameter	$P_{21/22}$	$P_{22/23}$	$P_{23/24}$
A	< 0	> 0	< 0
V_{sw}	442 km/s	416 km/s	360 km/s
B_e	5.5 nT	4.9 nT	3.9 nT
α	4.3°	4.3°	6.3°
a	0.03	0.03	0.02
b	0.02	0.02	0.01
d	0.5	0.5	1

Table 2. Neutron Monitors(NMs) and parameters used in the comparison for the last three solar minima.

NM	P_c (GV)	E_{eff} (GeV)	K_{NM} ($\text{m}^{-2}\text{sr}^{-1}\text{GeV}^{-1}$)
Apatity	0.65	6.50	3.16×10^{-5}
Oulu	0.80	6.54	3.53×10^{-5}
Yakutsk	1.65	6.87	3.43×10^{-5}
Moscow	2.43	7.41	2.07×10^{-5}
Novosibirsk	2.91	7.89	3.43×10^{-5}
Lomnický Stit	3.98	9.46	8.72×10^{-5}
Jungfraujoch	4.49	10.47	2.05×10^{-5}
Hermanus	4.58	10.67	2.63×10^{-5}
Rome	6.32	15.59	1.44×10^{-5}
Tbilisi	6.73	16.99	6.78×10^{-5}
Potchefstroom	7.00	17.96	2.69×10^{-5}

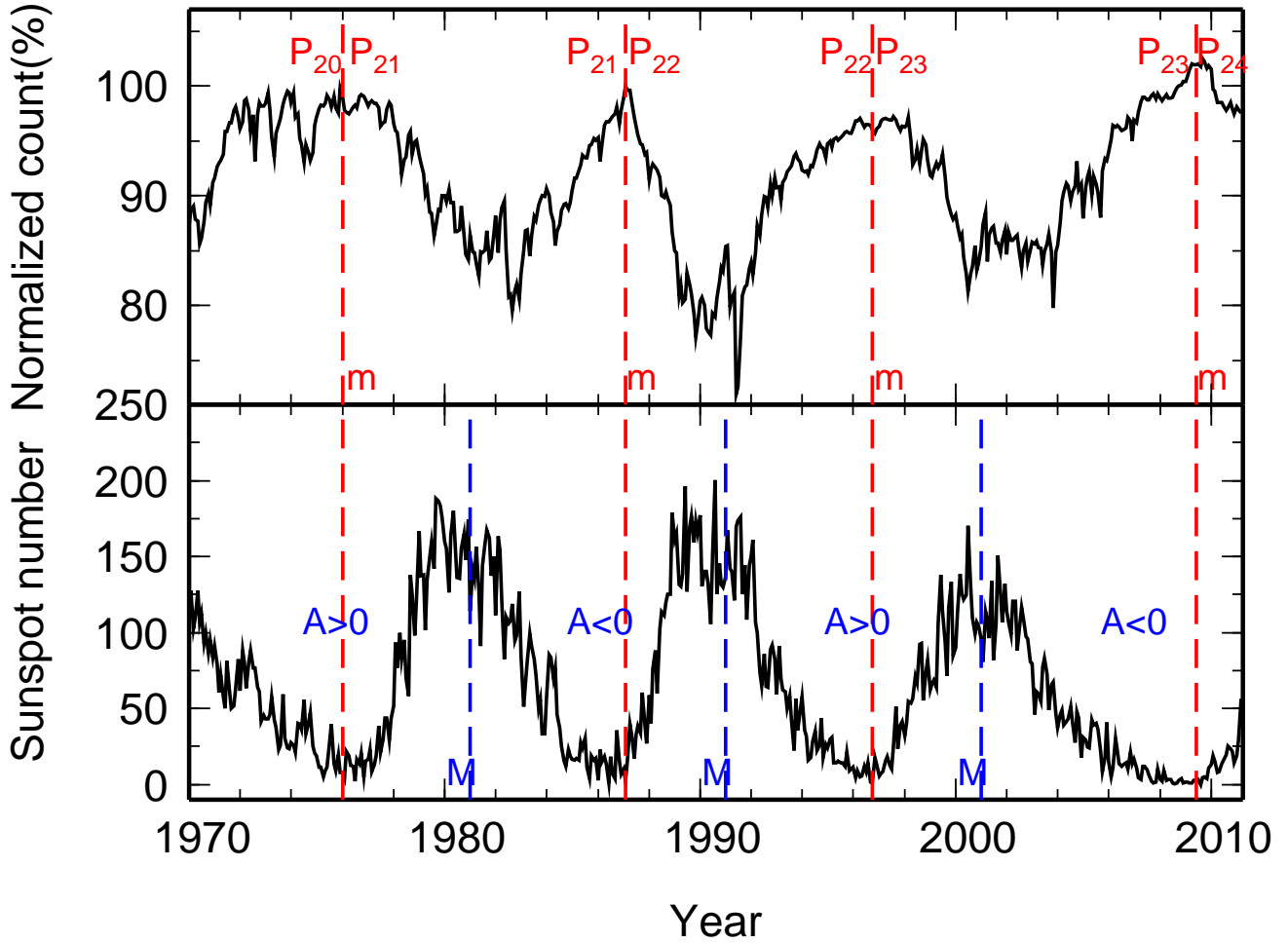


Figure 1. GCR intensity as measured by Apatity NM (upper panel) and monthly averaged SSN (lower panel). The red dashed-lines indicate the epochs of solar minima, and the red numbers represent solar cycles. The black dashed-lines indicate the epochs of solar maxima, and ‘ $A > 0$ ’ or ‘ $A < 0$ ’ represent the periods of solar magnetic polarity.

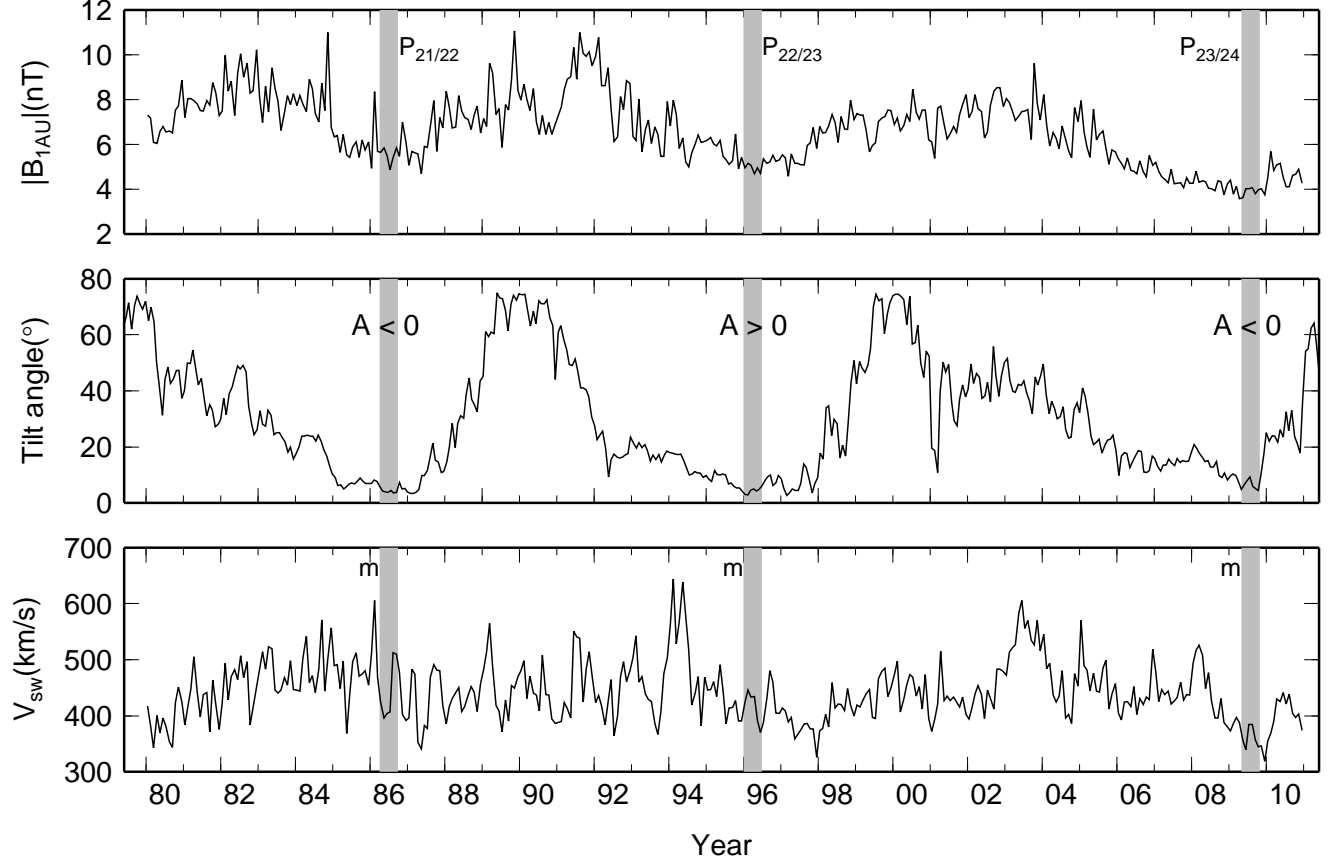


Figure 2. Temporal evolution interplanetary solar wind and magnetic field parameters measured at 1 AU. The IMF and SW speed are obtained by averaging the OMNI data over one-month intervals. The TA of the HCS is obtained from the WSO Web site with “new” model. The three grey shadow areas labeled with $P_{21/22}$, $P_{22/23}$ and $P_{23/24}$ indicate the three (21/22, 22/23, and 23/24) epochs of the solar minimum of approximately half a year long.

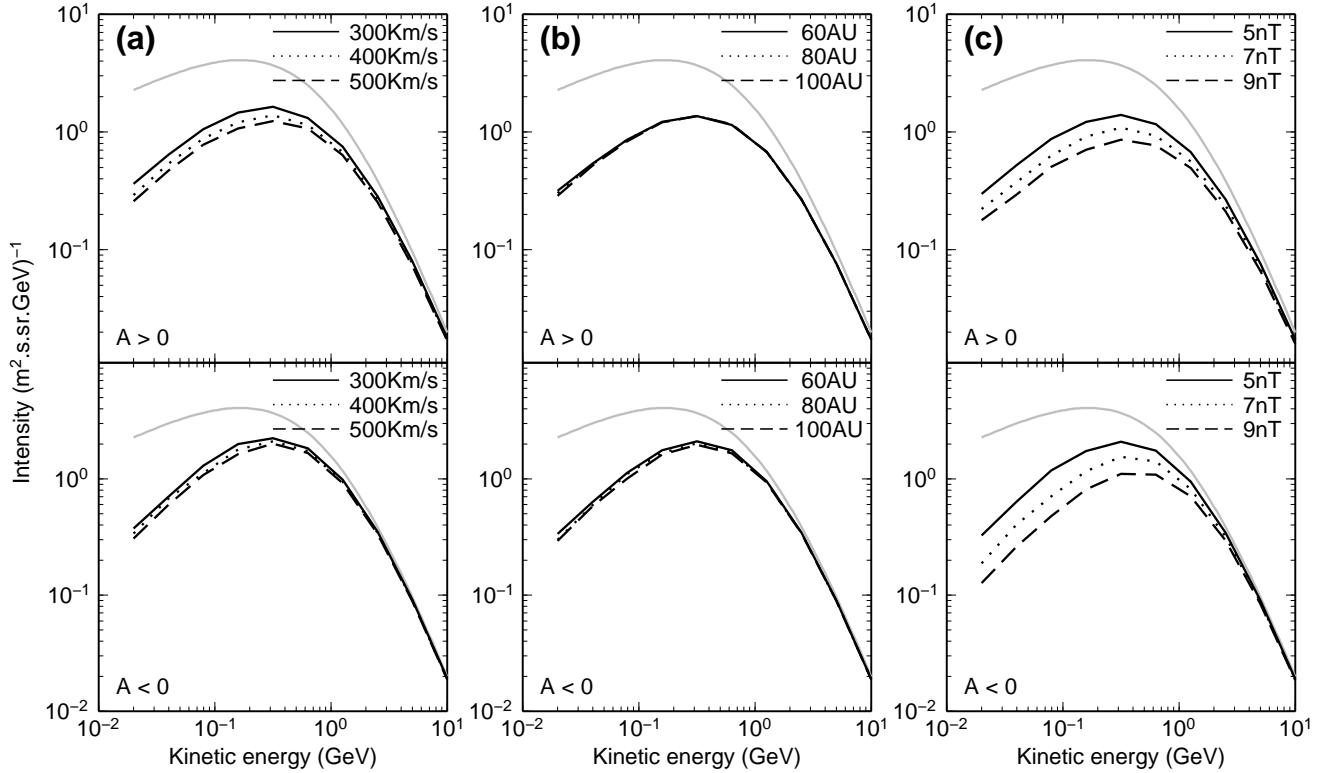


Figure 3. Computed differential intensity of GCR proton at Earth as a function of kinetic energy for both $A > 0$ and $A < 0$ magnetic polarities during the solar minimum condition with an unmodulated interstellar spectrum shown in grey line as a reference. Three different black lines indicate three assumptions for (a) SW speed, (b) distance of the outer heliospheric boundary, and (c) magnitude of IMF.

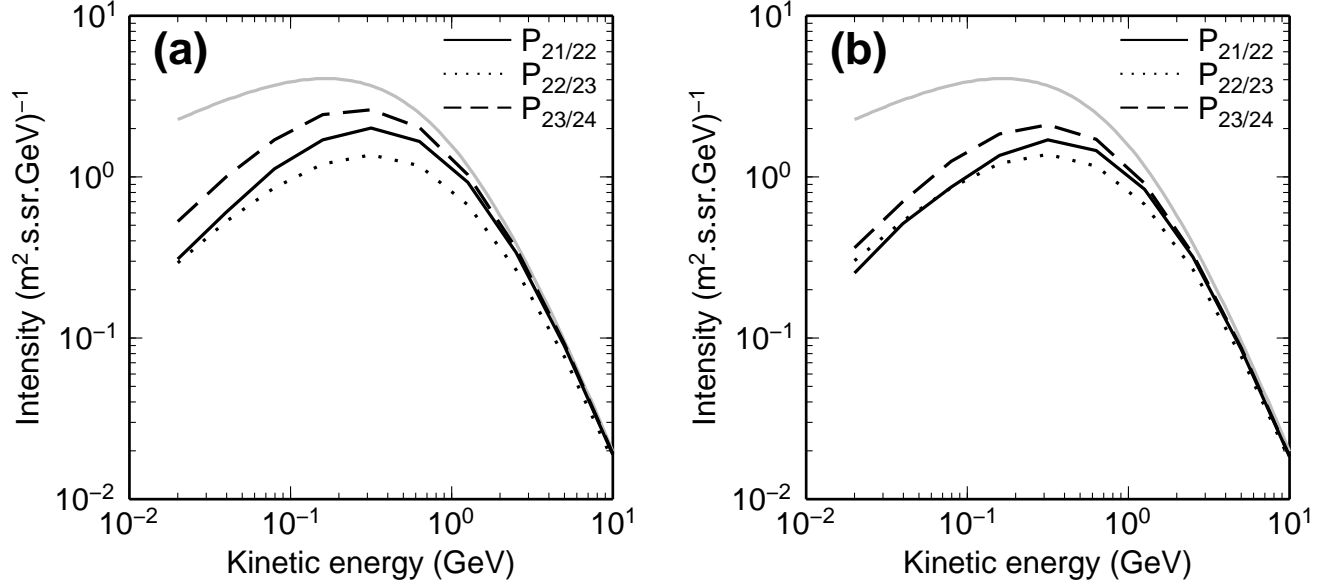


Figure 4. Computed GCR proton energy spectra at the Earth for different magnetic field strength B_e at Earth and SW speed V_{sw} with unmodulated interstellar spectrum shown in grey lines as a reference, during $P_{21/22}$ (dark solid line), $P_{22/23}$ (dotted line), and $P_{23/24}$ (dashed line). The TA of HCS is set to be (a) 0° and (b) the measured values during the corresponding periods.

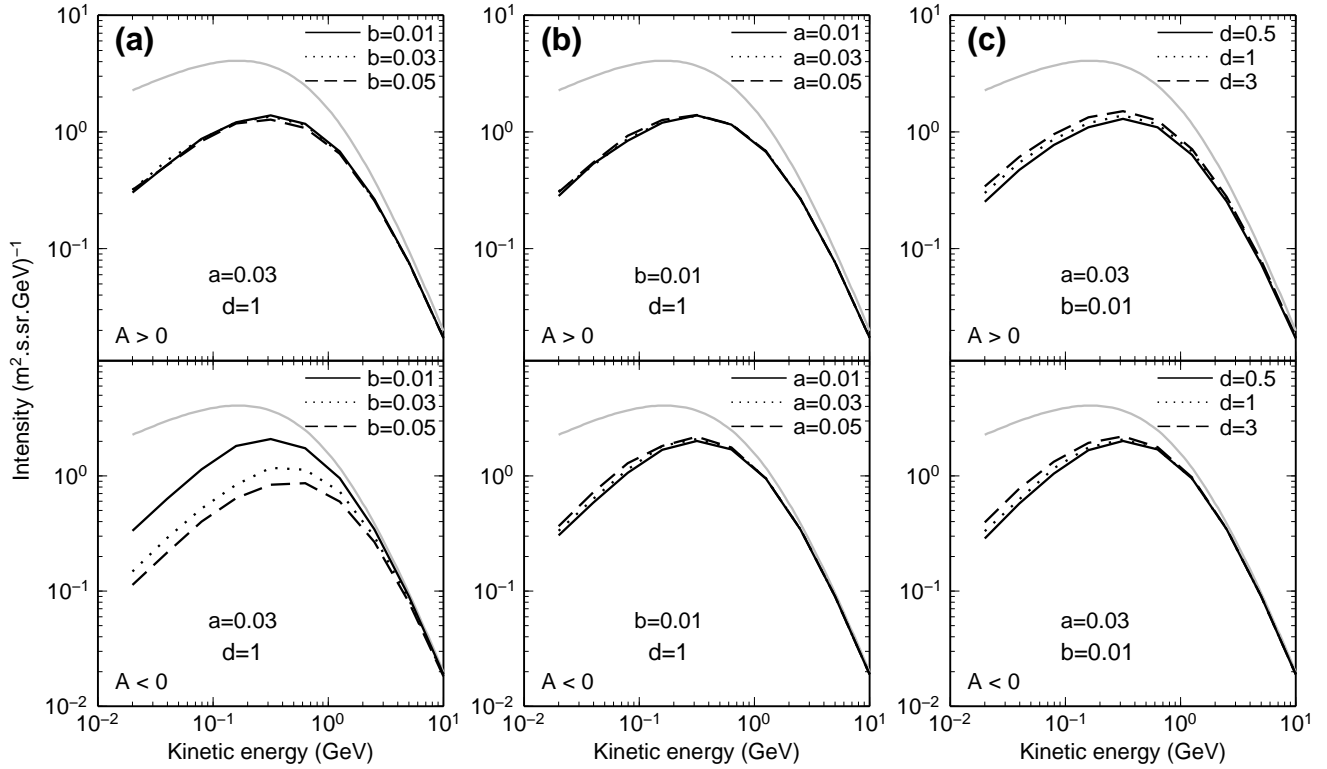


Figure 5. Computed differential intensity of GCR proton at Earth as a function of kinetic energy for both magnetic polarities during a solar minimum condition with unmodulated interstellar spectrum shown in grey lines as a reference. Three different black lines indicate three assumptions for (a) polar perpendicular diffusion factor b , (b) radial perpendicular diffusion factor a and (c) parallel diffusion factor d .

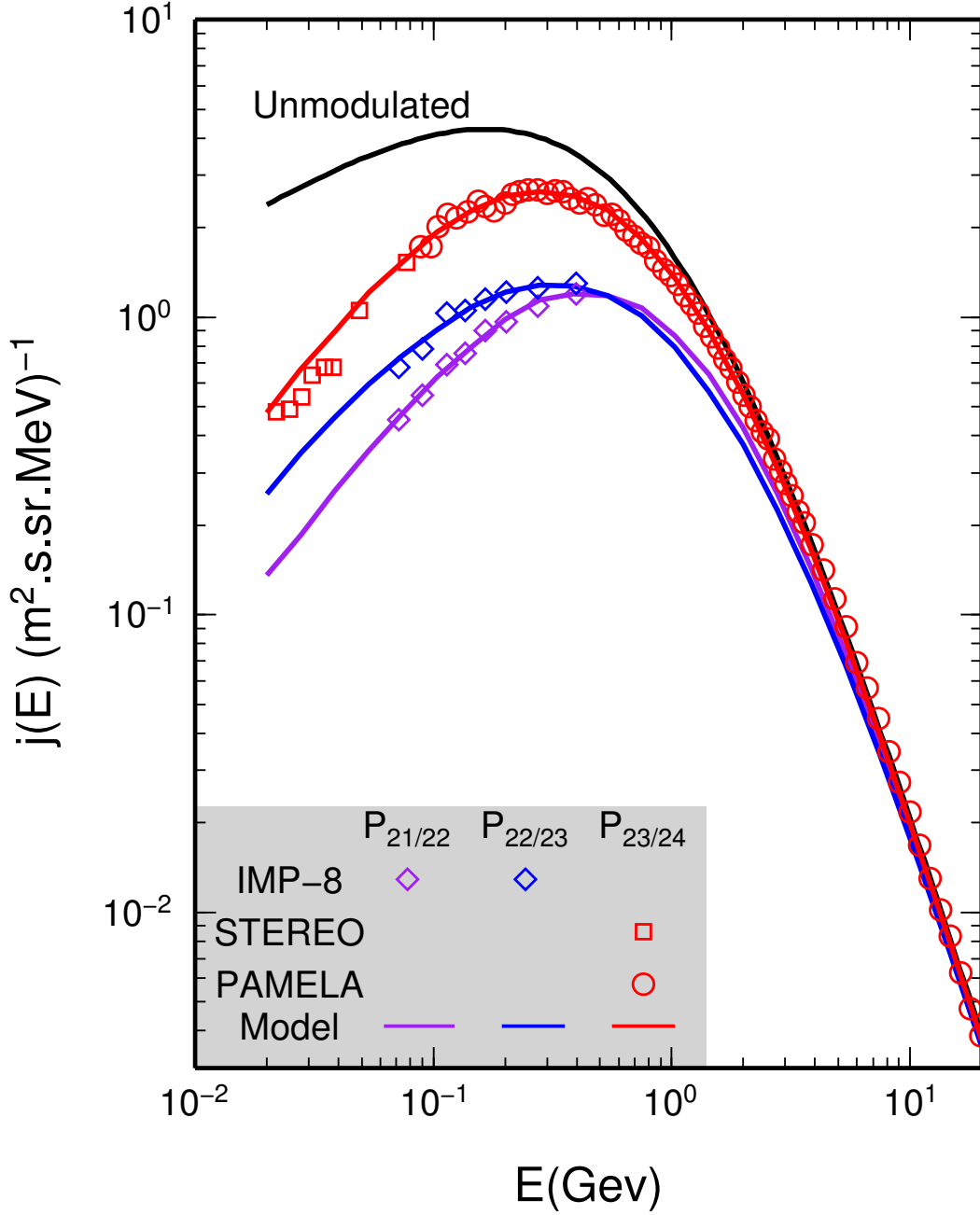


Figure 6. Computed GCR proton energy spectra at the Earth for the last three solar minima with parameters presented in table 1. The observation data are calculated from the measurements of proton flux by STEREO (squares) and IMP-8 (diamonds) after SEP contribution is removed. And red circles denote the measurements from PAMELA instrument for the year 2009 [Adriani *et al.*, 2013, table 1].

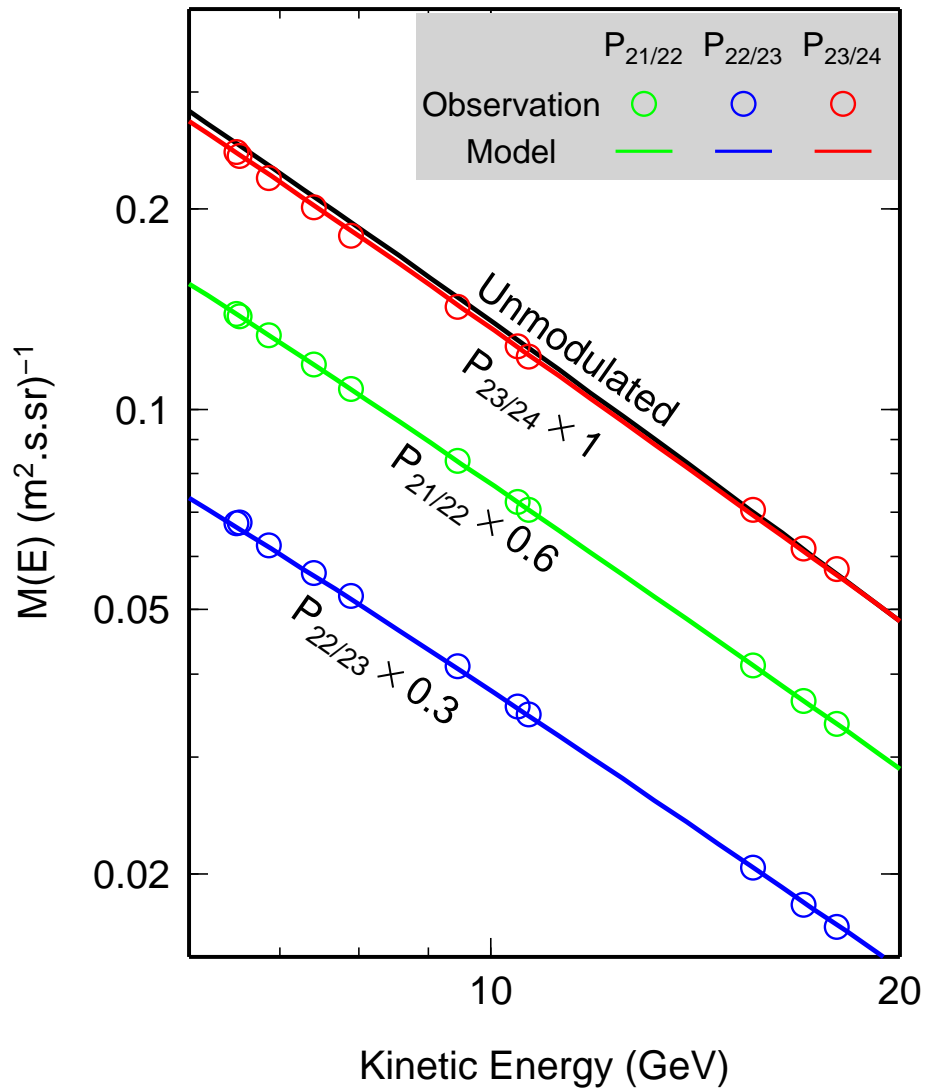


Figure 7. Comparison between the computed GCR integral flux and the NM count rates for the last three solar minima. Note that both simulation result and observation of each solar minimum are multiplied by an arbitrary factor as denoted in figure, for the purpose of presentation.

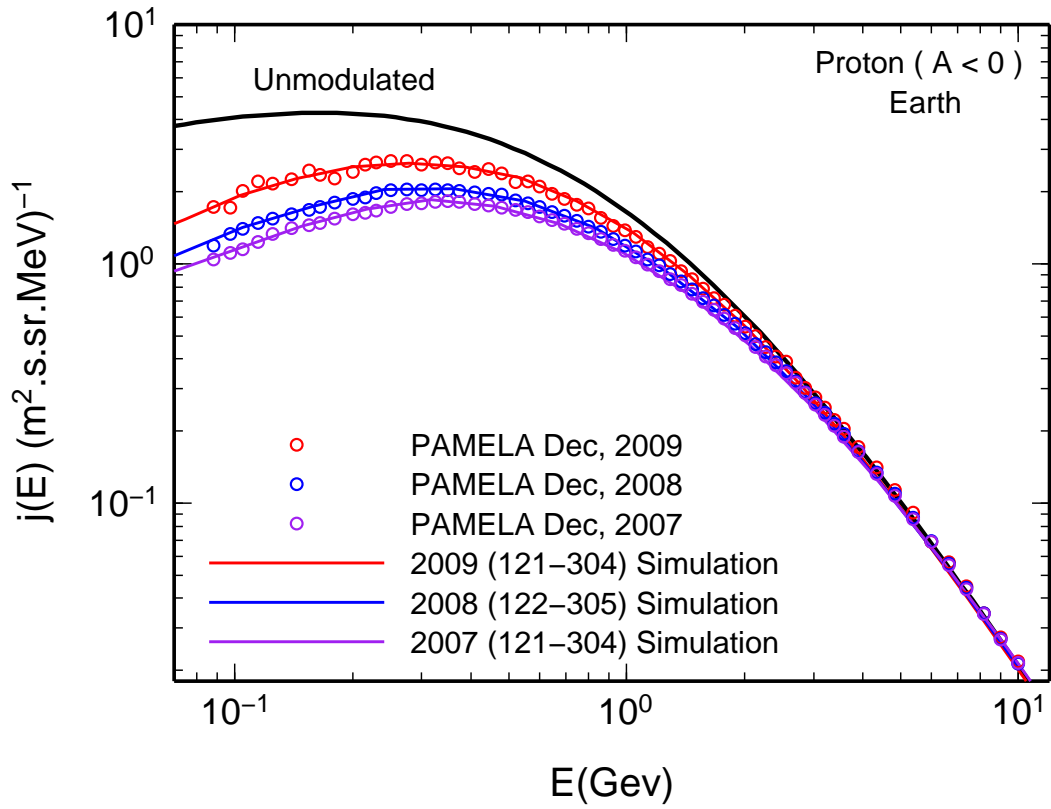


Figure 8. Evolution of the proton energy spectrum during the period of minimum solar activity, from year 2007 to year 2009. The purple, blue and red curves indicate the computed GCR proton differential fluxes corresponding to three half year periods, 2007 (121-304), 2008 (122-305), and 2009 (121-304), respectively. An unmodulated interstellar spectrum is shown in black line for reference. The observations from PAMELA instrument are also shown (circles).